frontiers | Frontiers in Astronomy and Space Sciences

TYPE Original Research
PUBLISHED 25 September 2024
DOI 10.3389/fspas.2024.1466975

OPEN ACCESS

EDITED BY
Tom Millar,
Queen's University Belfast, United Kingdom

REVIEWED BY
Helgi Rafn Hrodmarsson,
Laboratoire Inter-universitaire des Systemes Atmospheriques (CNRS UMR 7583)–Université Paris Est Créteil (UPEC), France
German Molpeceres De Diego,
Spanish National Research Council (CSIC), Spain

*CORRESPONDENCE
Ryan C. Fortenberry,
r410@olemiss.edu

RECEIVED 18 July 2024
ACCEPTED 09 September 2024
PUBLISHED 25 September 2024

CITATION
Firth RA and Fortenberry RC (2024) Alternate formation of AlOH from third row diatomic hydrides and oxides.
Front. Astron. Space Sci. 11:1466975.
doi: 10.3389/fspas.2024.1466975

Alternate formation of AlOH from third row diatomic hydrides and oxides

Rebecca A. Firth and Ryan C. Fortenberry*

Department of Chemistry and Biochemistry, University of Mississippi, Oxford, MS, United States

One of the most abundant Al-containing molecules detected in the interstellar medium (ISM) is AlOH. Over the past several years, there have been various pathways proposed for the formation of AlOH in the ISM, including reactions between AlO and H_2 or H_2O. However, these pathways include an energetic barrier from a transition state that likely prevents the reaction from progressing efficiently in the low temperature/low pressure environment of the ISM. Recently, a barrierless pathway for formation of AlOH from AlO and AlH has been proposed for the formation of AlOH. Even so, only one of these species really needs to contain an aluminum atom. To account for this, alternative but related pathways reacting the known interstellar molecule AlO with XH and AlH with XO (X = Mg, Si, P, or S) to form AlOH are explored with high accuracy quantum chemical calculations via CCSD(T)-F12b/cc-pVTZ-F12. Each third row element has at least one pair of reactants that lead to exothermic formation of AlOH. These reactions can go on to form other aluminum oxides and aluminum oxide clusters that may, in part, lead to the formation of interstellar dust grains.

KEYWORDS

reaction pathways, submerged barriers, aluminum chemistry, third row chemistry, diatomic reactants, coupled cluster theory

1 Introduction

Despite aluminum being the 11th most abundant element in the solar system (Asplund et al., 2009), aluminum levels in the interstellar medium (ISM) are still typically so low that this atom is not even considered "abundant" (Costantini et al., 2019). As aluminum-containing molecules are believed to be some of the first to form in circumstellar envelopes (CSEs) of AGB stars; a common hypothesis is that these aluminum molecules form corundum (Al_2O_3) and then larger complex dust grains (Clayton, 1978; Costantini et al., 2019). Aluminum being locked in dust grains would account for the low presence of gas-phase aluminum in the ISM. A possible starting material for corundum is AlOH. Current data shows AlOH to be one of the most abundant aluminum species in the CSEs of Al-rich AGB stars. However, the relative abundance of AlOH greatly depends on which region is being observed (Tenenbaum and Ziurys, 2010; Decin et al., 2017; Takigawa et al., 2017; Kamiński et al., 2016). The relative abundance of AlOH tends to be inversely related to the abundance of AlO, leading to the theory of AlO being involved in the formation of AlOH (Parnis et al., 1989; Sharipov et al., 2011; Mangan et al., 2021; Firth et al., 2024). AlO has been found in the CSEs of several O-rich AGB stars (Decin et al., 2017; Tachibana et al., 2019; Karovicova et al., 2013; Takigawa et al., 2017; Danilovich et al., 2020), suggesting the CSEs of these stars as a viable location for the initial steps of dust grain nucleation. In addition to AGB stars, AlO is also well known in cool (Kamiński et al., 2013) and variable

stars (Banerjee et al., 2003; Tylenda et al., 2005; Banerjee et al., 2012; Kamiński et al., 2016) as well as in sunspots (Sriramachandran et al., 2013). AlO has also been tentatively detected in the atmospheres of several exoplanet atmospheres (Bowesman et al., 2021) including the hot Jupiter exoplanets WASP-33b (von Essen et al., 2019), WASP-43b (Chubb et al., 2020), HAT-P-41n (Lewis et al., 2020; Sheppard et al., 2021), and the sub-Saturn KELT-11b (Colón et al., 2020). A recent proposed pathway of formation for AlOH from the reaction of AlO and AlH, shows a fully exothermic reaction with an Al atom as a leaving group (Firth et al., 2024). While this pathway is an improvement over prior methods of forming AlOH that include energetic barriers along the pathway (Parnis et al., 1989; Sharipov et al., 2011; Mangan et al., 2021), it heavily depends on limited quantities of aluminum as it requires two aluminum-containing species to produce a molecule containing only one aluminum atom. To remedy this, variations on this reaction are explored following the form of Equations 1, 2 below, where X = Mg, Si, P, or S:

$$\mathrm{AlH} + \mathrm{XO} \rightarrow \mathrm{AlOH} + \mathrm{X} \tag{1}$$

$$\mathrm{XH} + \mathrm{AlO} \rightarrow \mathrm{AlOH} + \mathrm{X}. \tag{2}$$

Again, where X = Al is partly the subject of Firth et al. (2024), and this motif follows that from previous work where dative bonding stabilizes the initial intermediate (Swinnen et al., 2009; Grosselin and Fortenberry, 2022). AlH has recently been observed in the atmosphere of our nearest stellar neighbor, Proxima Centauri (Pavlenko et al., 2022) and is well-known in sunspots (Wallace et al., 2000; Karthikeyan et al., 2010; Sotirovski, 1972) as well as the photospheres of other stars such as χ Cygni (Herbig, 1956; Johnson and Sauval, 1982). However, AlH has yet to be detected in interstellar gas (Pavlenko et al., 2022). This may be in part due to the small reduced mass of cold AlH pushing the rotational transitions to the submillimeter region (Pavlenko et al., 2022).

Of the alternate metals explored in this work, magnesium is the most common at the 8th most abundant element in the Universe (Rogantini et al., 2020). Despite this, the diatomic hydrides and oxides (MgH and MgO) have limited instances of detection. Optical spectra of bright mid-L dwarf stars obtained with the W. M. Keck Observatory show the presence of MgH as well as other metal hydrides and oxides (Kirkpatrick, 2005). Submillimeter observations of IRC + 10216 also show weak evidence of the MgH line (Avery et al., 1994). Recent work has also shown the possible existence of MgH in the atmosphere of the hot Jupiter HAT-P-41b (Jiang et al., 2024). Lastly, MgH has been see in sunspot spectra (Sotirovski, 1972) which suggests it could still be present in other stars (Yurchenko et al., 2017). MgO has also been observed in spectra of sunspots (Sotirovski, 1972), but there have been confirmed nondetections of MgO in IK Tau (Decin et al., 2018), R Dor (Decin et al., 2018), and a series of other O-rich AGB stars (Wallström et al., 2024) Both MgO and MgH are also considered to be important contenders for the molecular makeup of the atmospheres of hot super-Earth exoplanets (Tennyson and Yurchenko, 2017).

While silicon is less abundant than magnesium in the universe as the 9th most abundant element (Rogantini et al., 2020), there are still several instances of detection for SiH and SiO. Even though the diatomic hydride (SiH) has reported nondetections in IRC + 10216 (Siebert et al., 2020) and VY Canis Majoris (Siebert et al., 2020), there are tentative detections in both Orion-KL with use of the Caltech Submillimeter Telescope (Schilke et al., 2001) and in the solar disk spectrum (Sauval, 1969). SiH has also been found in the sun (Wöhl, 1971), implying it could still be present in other stars (Yurchenko et al., 2017). In contrast with SiH, SiO has been detected in a multitude of sources. SiO was initially detected in Sagittarius B2 (Wilson et al., 1971; Dickinson, 1972). Since the initial detection, SiO has also been detected toward diffuse interstellar molecular clouds (Lucas and Liszt, 2000; Turner, 1998), IRC + 10216 (Prieto et al., 2015), and in the CSEs of many O-rich AGB stars (Massalkhi et al., 2020). SiO is also theorized to be important in hot super-Earth exoplanet atmospheres (Tennyson and Yurchenko, 2017).

Phosphorus and sulfur are less abundant than magnesium, silicon, and aluminum. However, phosphorus is still one of the 20 most abundant elements in the solar photosphere (Caffau et al., 2011) and the known gaseous forms of sulfur only make up <1% of the elemental sulfur in the ISM (Kama et al., 2019; Costantini et al., 2019). Phosphorous hydride (PH) has not yet been detected, but PH is still theorized to exist. Reported nondetections of PH include observations of IRC + 10216 and VY Canis Majoris (Siebert et al., 2020). In contrast with PH, PO has been detected in several sources. PO Has been detected in the star-forming region L1157-B1 (Lefloch et al., 2016), the CSE of several O-rich AGB stars such as IK Tau (Ziurys et al., 2018; De Beck et al., 2013), R Cas (Ziurys et al., 2018), and TX Cam (Ziurys et al., 2018). The supergiant NML Cyg (Ziurys et al., 2018) has also shown signatures of the presence of PO. Additional studies on PO and other phosphorus-bearing molecules agree with the theory that phosphorus appears to be extremely depleted in inactive molecular gas by multiple orders of magnitude (Lefloch et al., 2016; Fontani et al., 2016; Rivilla et al., 2016). Sulfur has been detected in dust near C-rich AGB stars, planetary nebulae (Hony et al., 2002), and protoplanetary disks (Keller et al., 2002), primarily in the form of FeS (Costantini et al., 2019; Westphal et al., 2014). Other forms of sulfur have also been found in lower abundances. The diatomic hydride (SH) has been detected toward the submillimeter source W49N with SOFIA (Neufeld et al., 2012), while the oxide (SO) has been found in Orion KL as well as the CSEs of several O-rich AGB stars (Massalkhi et al., 2020). SO is also a contender for the molecular composition of atmospheres of hot super-Earth atmospheres (Tennyson and Yurchenko, 2017). Several other sulfur-containing molecules are also known (McGuire, 2018; McGuire, 2021), and this element has even been the subject of discussion for the so-called "missing sulfur" problem (Henry et al., 2004).

Beyond their abundances, chemical reactions in the inter- and circumstellar media have more limitations to be considered viable compared to reactions on Earth. For instance, bimolecular reactions become the primary contributors to chemical reactions due to the low number densities in these environments making it statistically unlikely for more than two molecules to collide at once (Puzzarini, 2022). The nature of these regions also prevents chemical reactions from accessing additional energy to overcome energetic barriers. This means that the only energy available for the reaction to occur is the energy from the initial starting materials (Tinacci et al., 2023). Due to this, the chemical reactions must also be exothermic

overall with an initial barrierless association of the starting materials (Puzzarini, 2022). The overall exothermic quality of the reactions, along with the low number densities, require a viable reaction to give off a leaving group to dispel the excess kinetic energy from the collision (Puzzarini, 2022). If there is no leaving group, the molecule must undergo vibrational relaxation to dispel the excess energy, or it will dissociate back to starting materials. The association of two molecules without the loss of a leaving group, radiative association, is considered note to be feasible as the probability of the molecules to simply fragment apart increases instead of them undergoing vibrational relaxation (Tinacci et al., 2023). Consequently, all of the reaction pathways discussed in this work are evaluated based on the requirements of viable reactions in the ISM/CSM as well as the abundance for each set of starting materials.

2 Computational methods

The reaction pathways explored in this work are based in the highly accurate CCSD(T)-F12b/cc-pVTZ-F12 level of theory, hereinafter referred to as F12-TZ. F12-TZ is based on coupled cluster theory at the singles, doubles, and perturbative triples level [CCSD(T)] (Raghavachari et al., 1989) along with the inclusion of the explicitly correlated F12b formalism (Adler et al., 2007; Knizia et al., 2009) in conjunction with the triple-ζ correlation consistent basis set cc-pVTZ-F12 (Hill and Peterson, 2010). The addition of the F12b formalism to the current "gold standard" CCSD(T) (Raghavachari et al., 1989; Hampel et al., 1992; Knowles et al., 1993; Deegan and Knowles, 1994; Helgaker et al., 2004) method allows for faster basis set convergence while producing higher-accuracy results with a basis set of the same order (Győrffy and Werner, 2018).

The starting materials, intermediate minima, and final products undergo a geometry optimization and harmonic frequency computation at the F12-TZ level of theory using the Molpro 2022.3, 2023.2, and 2024.1 quantum chemistry program suites (Werner et al., 2012). The harmonic zero-point vibrational energy is included in the total energy of the structure. Transition states along the pathway undergo a transition state optimization in Gaussian16 (Frisch et al., 2016) where a geometric structure and harmonic frequencies are computed. This transition state optimization is computed utilizing density functional theory (DFT) at the B3LYP/aug-cc-pVTZ (Dunning and Thom, 1989; Kendall et al., 1992; Woon et al., 1993) level of theory. The B3LYP computed geometry then undergoes a single-point energy (SPE) calculation via F12-TZ in Molpro to maintain consistent energies across the pathway for relative energy determination. The use of coupled cluster energies for DFT geometries has been previously shown not to affect greatly (less than 1 kcal mol^{-1} the energies for the coupled cluster comparison (Ramal-Olmedo et al., 2021; Ramal-Olmedo et al., 2023a; Ramal-Olmedo et al., 2023b; Nguyen et al., 2020). For transition states, the B3LYP computed harmonic zero-point energy is added to the F12-TZ energy from the SPE computation to determine the vibrationally-corrected energies. Intermediates along the pathway are located with the use of the motif shown in Firth et al. (2024). Relative energies included on the pathways are computed relative to one pair of starting materials for each pathway.

3 Results and discussion

3.1 Magnesium

Figure 1 shows the pathways to create AlOH from combinations of both sets of magnesium-bearing reactants: AlH/MgO and MgH/AlO. The MgH/AlO pair is lower in energy by 23.6 kcal mol^{-1} compared to the AlH/MgO pair. This is the smallest relative energy gap for all sets of reactants explored in this work. The relative energies in Figure 1 are relative to MgO/AlH. Beginning with the higher energy reactants, MgO and AlH are able to combine to form *c*−HAlMgO with 100.1 kcal mol^{-1} of stabilization or HAlOMg with 102.8 kcal mol^{-1} of stabilization. If *c*−HAlMgO is formed first, it can proceed through a low-barrier transition state at only −96.9 kcal mol^{-1} (3.2 kcal mol^{-1} higher) to open the ring and form HAlOMg. This transition state pulls the magnesium atom out of the plane as HAlOMg is formed. From here, the hydrogen can either shift to the oxygen, or the magnesium can dissociate to form linear HAlO. If the hydrogen shifts, the AlOH−Mg van der Waals complex is created before the magnesium dissociates with a 0.1 kcal mol^{-1} penalty to form AlOH. If the magnesium comes off earlier, the transition state to move the hydrogen to the oxygen lies only 24.0 kcal mol^{-1} below the reactants before forming AlOH.

If the lower energy reactants are present instead, there are two possible intermediates depending on the orientation of AlO. Both of these structures (HMgAlO and HMgOAl) are completely linear, though the relative energies are vastly different. HMgOAl has significantly more stabilization from the additional oxygen−metal bond and sits at −133.3 kcal mol^{-1} (109.7 kcal mol^{-1} below the reactants), whereas the Al−Mg metal−metal bond puts HMgAlO at −75.4 kcal mol^{-1} (only 51.8 kcal mol^{-1} of stabilization). HMgOAl is, then, able to transfer the hydrogen over to the oxygen and create a van der Waals complex AlOH−Mg before the magnesium fully dissociates with an increase in energy of only 0.1 kcal mol^{-1}, the same final step of forming AlOH as the higher-energy reactants produce. On the other hand, HMgAlO is able to transfer the hydrogen over to the aluminum to create *c*−HAlMgO, once again at −100.1 kcal mol^{-1} (76.6 kcal mol^{-1} below the reactants). *c*−HAlMgO is then able to proceed to AlOH as described previously. However, the magnesium is much more likely to dissociate at the very end as the transition state for HAlO is at −24.0 kcal mol^{-1} (only 0.4 kcal mol^{-1} below the energy of MgH and AlO). Additionally, the HMgOAl_TS was run via F12-TZ in Molpro for comparison to the aforementioned transition state methodology. As shown in Figure 1, the vibrationally-corrected energy for this transition state computed with a B3LYP geometry optimization followed by a F12-TZ SPE is −72.1 kcal mol^{-1} with respect to the AlH/MgO reactant pair. In comparison, the full F12-TZ geometry optimization gives a relative energy of −72.2 kcal mol^{-1}. This deviation of only 0.1 kcal mol^{-1} indicates there is not a significant difference between the F12-TZ and B3LYP geometries. These comparably accurate results and the greater efficiency of the Gaussian optimizer justify the use of this protocol, and as such the B3LYP optimization + F12-TZ SPE methodology will be retained for all other transition state computations. Finally, exploration of the MgH + AlO pathway utilizing M06-2X (Zhao and Truhlar, 2007) in place of B3LYP produces relative energies within 0.2 kcal mol^{-1} or less for all stationary points save for the last intermediate which varies by

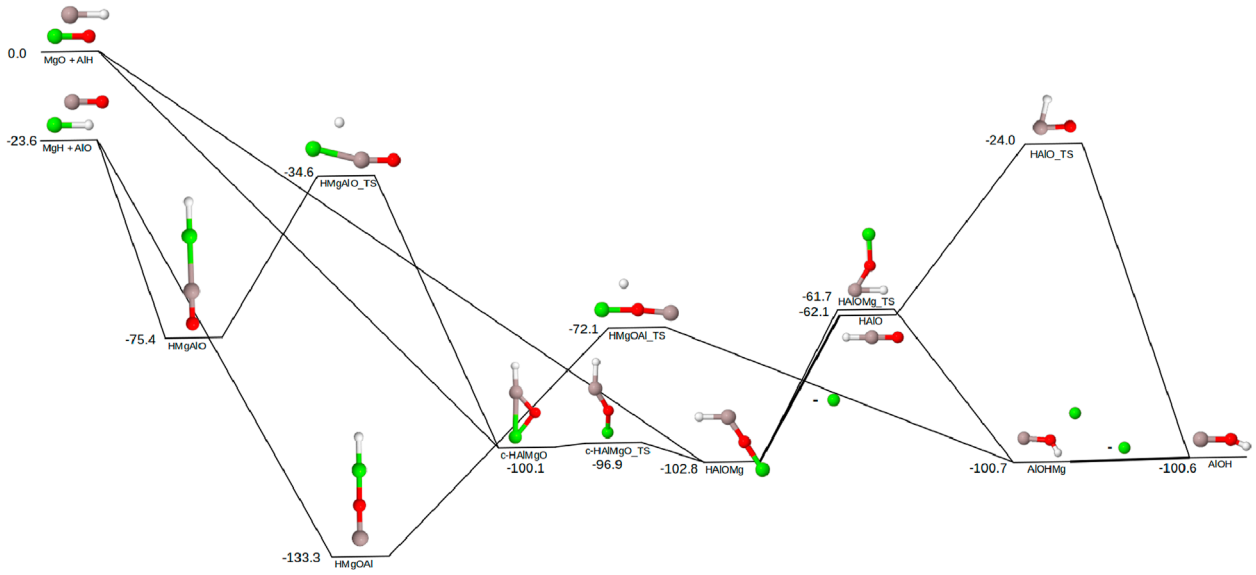

FIGURE 1
Reaction pathway for the formation of AlOH from AlO + MgH and AlH + MgO. Relative energies are expressed in kcal mol^{-1}. Color scheme as follows: Al (grey), Mg (green), O (red), H (white). Lines on the pathway are bold where the Mg dissociation occurs. All molecules in this pathway are singlets except for MgH and AlO which are both doublets.

0.7 kcal mol^{-1}. Regardless, the choice of functional does not greatly affect the final energetic outcomes.

3.2 Silicon

The reaction pathways for the formation of AlOH with the silicon reactant pairs (SiH/AlO and SiO/AlH) are shown in Figure 2. In contrast with the magnesium reactants, the SiO/AlH pair is significantly lower in energy with a difference of 65.7 kcal mol^{-1} between the two sets of reactants. The relative energies in Figure 2 are determined relative to SiH/AlO. When considering, first, the reactant pair of SiO/AlH, the intermediates *c*–HAlOSi and HAlOSi can form with relative energies of −93.7 and −77.0 kcal mol^{-1} (28.0 and 11.3 kcal mol^{-1} below SiO/AlH), respectively. These intermediates and the transition state between them are very similar to the respective magnesium structures with a few differences. For instance, the ring structure *c*–HAlOSi has the hydrogen bent toward the oxygen instead of creating a linear angle in the Mg-analog of this structure. As with the Mg-analog, the transition state of the ring opening has the Si-atom bending out of the plane to form HAlOSi in C_1 symmetry. It should also be noted that while the Mg-analogs of these structures have the cyclic form higher in energy than the open HAlOMg, the silicon structures have the *c*–HAlOSi lower in energy than the open HAlOSi. Once HAlOSi has been formed, the same options as with the magnesium structures are available. If the silicon atom is lost before the hydrogen shifts onto the oxygen, the HAlO structure lies at 1.3 kcal mol^{-1} (67 kcal mol^{-1} above the SiO/AlH reactants), making this route impossible without an external source of energy. If the hydrogen migrates before losing the silicon, the energy of the H-migration transition state also exceeds the energy of SiO/AlH by 42.1 kcal mol^{-1}. This, along with the AlOH/Si product being higher in energy than SiO/AlH, shows that the combination of SiO/AlH will not be able to form AlOH without an external source of energy.

If, instead, the SiH/AlO reactant pair is considered, the orientation of AlO produces two possible intermediate structures (HSiAlO and HSiOAl). The creation of an Si–O bond in HSiOAl results in a very strong stabilization effect of 114.8 kcal mol^{-1}. The transition state for the H-migration from the silicon to the oxygen costs 85.3 kcal mol^{-1} of energy before creating the AlOHSi ring structure. The silicon atom can then fall off and produce AlOH. The AlOH/Si products lie 37.2 kcal mol^{-1} below the energy of the SiH/AlO reactant pair. If the orientation of AlO is such that a Si–Al bond is created instead, there is still 47.2 kcal mol^{-1} of stabilization. The transition state to migrate the hydrogen onto the aluminum atom and form *c*–HAlOSi stays below the energy of the initial reactants. However, it approaches the energy of SiH/AlO with only a −2.5 kcal mol^{-1} difference. Once *c*–HAlOSi has been formed, the molecule is able to follow the path previously described to ultimately form the AlOH/Si product. The increased starting energy allows for the rearrangement from HAlOSi to AlOHSi to occur energetically. The alternate path of losing the Si-atom early still exceeds the energy of SiH/AlO and will not be able to occur.

3.3 Phosphorus

Possible reaction pathways for the formation of AlOH with the phosphorus-containing reactant pairs (PH/AlO and PO/AlH) are shown in Figure 3. The phosphorus reactant pairs follow a similar pattern to the silicon pairs with the PO/AlH pair existing 44.1 kcal mol^{-1} lower in energy than PH/AlO. Both reactant pairs for phosphorus follow similar motifs as both Mg and Si, with a couple

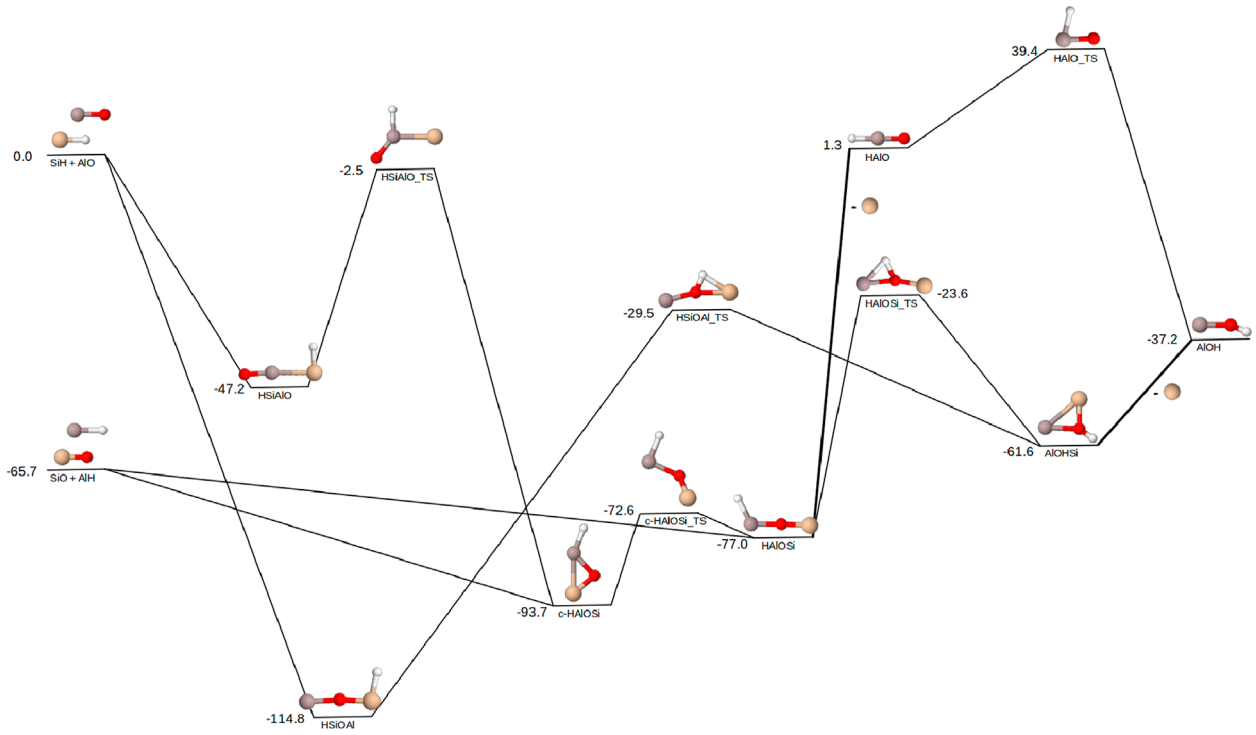

FIGURE 2
Reaction pathway for the formation of AlOH from AlO + SiH and AlH + SiO. Relative energies are expressed in kcal mol^{-1}. Color scheme as follows: Al (grey), Si (tan), O (red), H (white). Lines on the pathway are bold where the Si dissociation occurs. All molecules in this pathway are singlets except for SiH and AlO which are both doublets.

differences as well as additional routes of formation for AlOH/P. The product pair is lower in energy than both sets of reactants, suggesting it will be thermodynamically possible to create AlOH/P from both sets of starting materials. As with silicon, loss of the phosphorus atom too early pushes the energy of the system above the energy of the reactants, which makes this route not ideal for interstellar or circumstellar reactions.

In comparing the phosphorus reaction pathways to those previously shown for silicon and magnesium, the *c*–HAlOP to HAlOP section is very similar to the *c*–HAlOSi to HAlOSi section of Figure 2. The most notable differences is that the transition state remains planar for the P-analog. As with the Si-analogs of these structures, *c*–HAlOP is more stable than the open HAlOP structure. For the first time, there is another structure that can form between the PO/AlH reactants and *c*–HAlOP. This structure, HAlPO, lies at −63.9 kcal mol^{-1} (19.8 kcal mol^{-1} below PO/AlH) and is able to undergo a ring-closing transition state only 1.1 kcal mol^{-1} above HAlPO to form *c*–HAlOP. The *c*–HAlOP structure is also able to undergo a hydride shift from the Al to the O in order to move straight to AlOHP, which does not occur in the Mg and Si reaction pathways. The transition state for this hydride shift is higher in energy than the ring opening transition state by 16.8 kcal mol^{-1}. However, the hydride shift remains 5.7 kcal mol^{-1} below the energy of the PO/AlH reactants as opposed to the hydride shift after forming HAlOP, which exceeds the reactant energy by 15.6 kcal mol^{-1}. The earlier hydride shift allows the full process to form AlOH/P from PO/AlH to stay below the energy of the reactants. This is the only energetically favorable path from *c*–HAlOP to AlOH/P.

When starting with the PH/AlO reactants instead, there is once again very strong stabilization from the addition of these reactants. HPOAl is able to follow the same motif of a hydrogen migration followed by the loss of a phosphorus atom to form AlOH/P. Additionally, HPAlO is able to follow the same previously discussed hydrogen migration and ring closing mechanism to form *c*–HAlOP and then proceed on to eventually form AlOH/P. HPAlO is also able to bend such that the hydrogen migrates onto the oxygen in one step to form PAlOH. The transition state for this process exists 13.9 kcal mol^{-1} lower than the transition state to form *c*–HAlOP. The phosphorus can then dissociate from PAlOH to form AlOH/P with a loss of 30.1 kcal mol^{-1} of energy.

3.4 Sulfur

Finally, the reaction pathways for the sulfur-containing reactant pairs SO/AlH and SH/AlO are shown in Figure 4. The sulfur reactant pairs follow the same pattern as the magnesium pairs with the SH/AlO pair 35.4 kcal mol^{-1} lower in energy than SO/AlH. Both sets of reactant pairs are able to follow the motifs present in the phosphorus pathway (Figure 3). Beginning with the reactions of SH/AlO, the initial intermediates, HSOAl and HSAlO, are flipped energetically compared to the analogs with Mg, Si, and P. Where previously the species with the terminal aluminum would be lower in energy, the S-analog shows the terminal oxygen as 15.7 kcal mol^{-1} lower in energy. This could be due to oxygen and sulfur both being in the chalcogen family and their strong propensity to form bonds

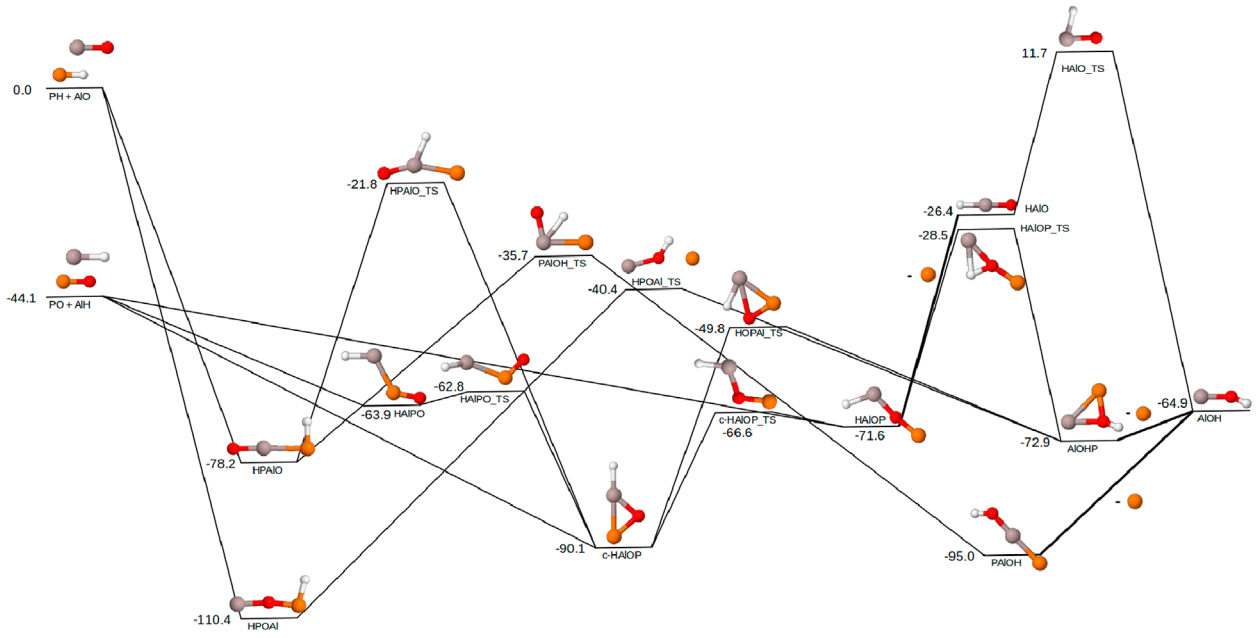

FIGURE 3
Reaction pathway for the formation of AlOH from AlO + PH and AlH + PO. Relative energies are expressed in kcal mol^{-1}. Color scheme as follows: Al (grey), P (orange), O (red), H (white). Lines on the pathway are bold where the P dissociation occurs. All molecules in this pathway are doublets except for PH, AlH, and AlOH which are singlets.

with one another (Doerksen and Fortenberry, 2020). The similar chemistry between these two elements minimizes the stabilization effects of the additional bond with oxygen shown in Figures 1–3. Both HSOAl and HSAlO are able to proceed on to form AlOH/S without exceeding the initial energy of SH/AlO. The hydrogen migration transition states to move the hydrogen onto the oxygen are both ~40 kcal mol^{-1} above the energy of the respective intermediate structure. It should be noted that unlike in the phosphorus pathway, HSAlO does not form *c*–HAlOS. The molecule, instead, bends to move the hydrogen all the way over to the oxygen in one step. A scan of the bending coordinate in this manner at step sizes of 2° confirms that no minima exist on this pathway. Additionally, the AlOHS structure preceding the loss of a sulfur atom differs from the Si/P-analogs by the C_1 symmetry as opposed to the C_s symmetry of the Si/P-analogs.

Depending upon the orientation of the reactants when SO and AlH collide, there are three possible initial intermediates: HAlSO, *c*–HAlOS, or HAlOS at −42.4, −86.6, and −53.1 kcal mol^{-1} respectively. As with the phosphorus pathway, HAlSO precedes *c*–HAlOS. The transition state to close the ring and form *c*–HAlOS is even more low-lying than the P-analog at only 0.7 kcal mol^{-1} above HAlSO. *c*–HAlSO can then open to form HAlOS. As is the case with the Mg/Si-analogs, this ring-opening transition state (*c*–HAlSO_TS) bends out of the plane of the molecule. This transition state has a very shallow potential as it only lies 0.1 kcal mol^{-1} higher than HAlOS. HAlOS and *c*–HAlOS can both undergo a hydrogen migration to form AlOHS and ultimately lose the sulfur atom. As shown previously with Si and P, losing the S atoms before the penultimate intermediate structure causes the hydrogen migration to form AlOH from HAlO to exceed the energy of the reactants by 16.7 kcal mol^{-1}. As long as the sulfur loss occurs as the last step, all of the hydrogen migration transition states and subsequent intermediates exist at least 22.8 kcal mol^{-1} under the energy of SO/AlH.

4 Astrophysical implications

Based on the previously discussed detections of the initial diatomics, MgH has a known presence in a variety of locations while MgO has yet to be detected in regions of high dust nucleation. This suggests MgH and AlO as the more likely pair of starting materials for AlOH creation in this manner. However, MgO and AlH cannot be discounted completely as the difficulty in detecting MgO could be related to MgO quickly reacting in the manner described here or creating larger magnesium structures such as Mg_2O (Costantini et al., 2019; Flint et al., 2024). In the event these AlH/MgO and MgH/AlO reactants are present in a high-temperature region, such as the atmosphere of a hot exoplanet, the reactions in Figure 1 will likely still occur. The higher temperature will provide the reactants more energy to cascade through the pathways, submerging the barriers even further below the energy of the reactants.

While SiO is observed more readily than SiH in circumstellar and interstellar regions, SiO is so low in relative energy (Figure 2) that it will likely not contribute to the formation of AlOH. Thus, SiO is likely to participate in the formation of larger silicates instead of AlOH (Flint and Fortenberry, 2023). While SiH has fewer instances of detection than SiO, SiH has been found in locations where AlO has also been detected such as VY Canis

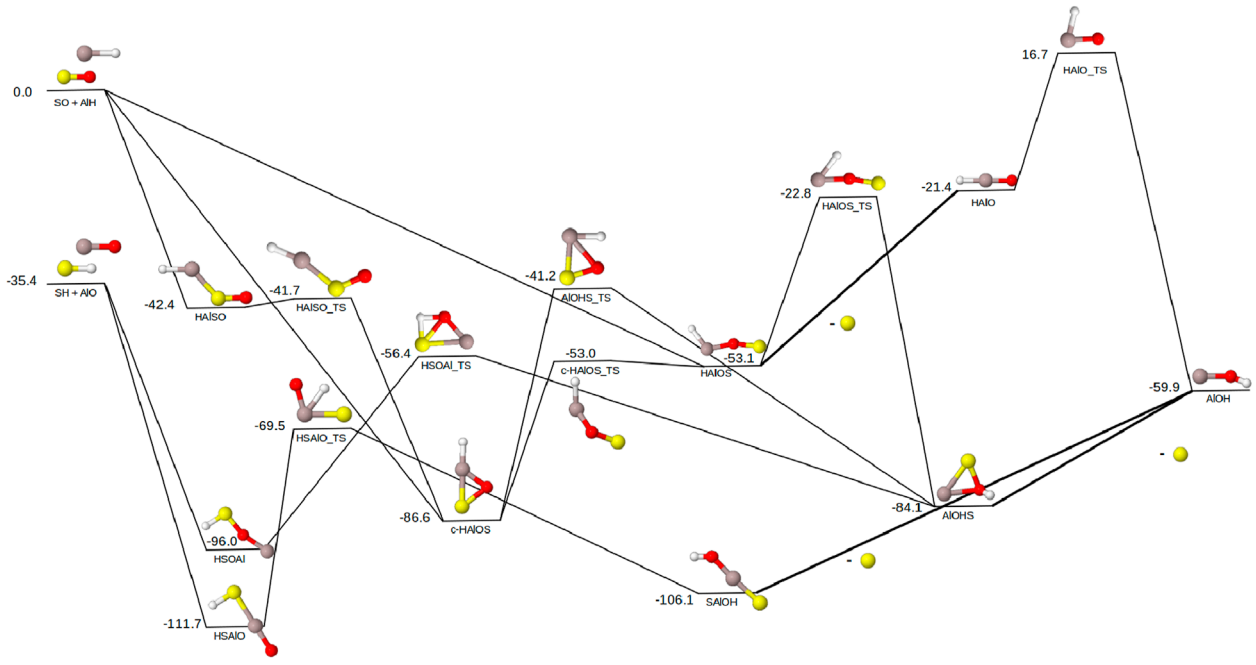

FIGURE 4
Reaction pathway for the formation of AlOH from AlO + SH and AlH + SO. Relative energies are expressed in kcal mol^{-1}. Color scheme as follows: Al (grey), S (yellow), O (red), H (white). Lines on the pathway are bold where the S dissociation occurs. All molecules in this pathway are singlets except for SH and AlO which are both doublets.

Majoris (Tenebaum and Ziurys, 2009). This, along with the lone energetically favorable path of formation stemming from SiH, suggests reactions of SiH with AlO to be the most likely method to form AlOH with silicon diatomics. SiH has also been the focus of other theoretical reaction pathways including the possible formation of SiS (Fortenberry and McGuire, 2024), and detection of molecules in pathways where it could be invoked imply its (as-of-yet undetected) presence. High temperature environments such as hot and ultra-hot exoplanets can reach temperatures up to and exceeding 2,500 K (Garhart et al., 2020; Baxter et al., 2020; Jones et al., 2022), which could potentially provide sufficient energy to the reactants to overcome the barriers. A Boltzmann population analysis indicates a temperature of 4,600 K would be requisite to provide enough energy to the SiO/AlH reactants for 1% of the reactants to surpass the energy barriers shown in Figure 2 and form AlOH. Along a similar vein, for 1% of the HAlO intermediate to surpass the HAlO_TS barrier and form AlOH, the environment would need to be at a temperature of 4,200 K. The most extreme member of the ultra-hot Jupiter classification and the hottest known exoplanet to date is KELT-9b with an equilibrium temperature of 4,050 ± 180 K (Jones et al., 2022; Gaudi et al., 2017) As the barriers present in the Si pathways are so large as to require temperatures over 4,000 K to form an appreciable amount of product, the high temperatures are unlikely to have a significant impact on the viability of these reactions unless the reactions are taking place in an environment as hot as KELT-9b. In general, the main contribution from elevated temperatures in hot exoplanets is simply providing the reactants with more energy to proceed through the pathways already containing fully submerged barriers.

The complete lack of detection of PH suggests that the PO/AlH reactants will be more likely to react and form AlOH. However, the nondetections of PH could be due to the hydride reacting extremely quickly to form larger structures. Hence, the PH/AlO reactants should not be fully discounted. The PO/AlH reactants show a pathway that prevents the formation of AlOH with the HAlOP_TS barrier 15.6 kcal mol^{-1} above the energy of the PO/AlH reactants. According to a Boltzmann population analysis, this barrier is small enough for temperatures of 1,700 K to allow for 1% of the reactants to surpass the barrier and form AlOH. Hot Jupiters have equilibrium temperatures in the range of 1,500–2,000 K (Baxter et al., 2020), suggesting such exoplanets as suitable environments for the PO/AlH reactants to progress through the *c*–HAlOP intermediate toward AlOH, presuming PO and AlH are both present.

The detections of both SH and SO support the viability of each set of reactants to form AlOH. While much of the sulfur in space is believed to be tied up in FeS (Costantini et al., 2019), the likelihood of the sulfur reactants participating in the formation of AlOH is lower than the magnesium or silicon reactants. However, the greater understanding of how SH and SO react with other species will aid in future studies of the sulfur diatomics in inter- and circumstellar regions, such as the proposed formation of SiS using SH (Fortenberry and McGuire, 2024).

5 Conclusion

This work proposes a series of gas-phase routes of formation for AlOH in CSEs of AGB stars from a combination of third row

diatomic hydrides and oxides. Nearly every combination of reactants explored has at least one energetically favorable route of formation to the AlOH/X products. Each pathway follows a series of similar motifs for the rearrangements while the phosphorus and sulfur pathways begin to add more paths that are unavailable to magnesium and silicon. In truth AlOH is likely formed from a mixture of these pathways depending upon the abundance of various required starting materials. While some of the proposed reactants have not yet been identified in CSEs or other astronomical regions of space, these reactions can not be completely discounted as the abundances of those diatomics may be low due to quick reactions to form other species. Future kinetic studies are necessary to determine the rates of the rearrangements occurring during these proposed reaction pathways and predict the fastest path. Additional observations of AGB stars where some of these diatomic molecules could exist are crucial to try to confirm the existence of these diatomics in such environments.

Data availability statement

The original contributions presented in the study are included in the article/Supplementary Material, further inquiries can be directed to the corresponding author.

Author contributions

ReF: Conceptualization, Data curation, Formal Analysis, Investigation, Methodology, Validation, Visualization, Writing–original draft, Writing–review and editing. RyF: Conceptualization, Data curation, Funding acquisition, Methodology, Project administration, Resources, Supervision, Validation, Writing–review and editing.

Funding

The author(s) declare that financial support was received for the research, authorship, and/or publication of this article. This work is funded through NASA Grants NNH22ZHA004C and 22-A22ISFM-0009 as well as the University of Mississippi's College of Liberal Arts and Graduate School. The Mississippi Center for Supercomputing Research funded in part by NSF grant OIA-1757220 provided the computational hardware needed for this work.

Conflict of interest

The authors declare that the research was conducted in the absence of any commercial or financial relationships that could be construed as a potential conflict of interest.

The author(s) declared that they were an editorial board member of Frontiers, at the time of submission. This had no impact on the peer review process and the final decision.

Publisher's note

Supplementary material

The Supplementary Material for this article can be found online at: https://www.frontiersin.org/articles/10.3389/fspas.2024.1466975/full#supplementary-material

References

Adler, T. B., Knizia, G., and Werner, H.-J. (2007). A simple and efficient CCSD(T)-F12 approximation. *J. Chem. Phys.* 127, 221106. doi:10.1063/1.2817618

Asplund, M., Grevesse, N., Jacques, S. A., and Scott, P. (2009). The chemical composition of the sun. *Annu. Rev. Astron. Astrophys.* 47, 481–522. doi:10.1146/annurev.astro.46.060407.145222

Avery, L. W., Bell, M. B., Cunningham, C. T., Feldman, P. A., Hayward, R. H., McLeod, J. M., et al. (1994). Submillimeter molecular line observations of IRC +10216: searches for MgH, SiH_2, and HCO^+, and detection of hot HCN. *Astrophys. J.* 426, 737. doi:10.1086/174110

Banerjee, D. P. K., Varricatt, W. P., Ashok, N. M., and Launila, O. (2003). Remarkable changes in the near-infrared spectrum of the nova-like variable V4332 sagittarii. *Astrophys. J.* 598, L31–L34. doi:10.1086/380389

Banerjee, D. P. K., Varricatt, W. P., Mathew, B., Launila, O., and Ashok, N. M. (2012). The A-X infrared bands of aluminum oxide in stars: search and new detections. *Astrophys. J. Lett.* 753, L20. doi:10.1088/2041-8205/753/1/L20

Baxter, C., Désert, J.-M., Parmentier, V., Line, M., Fortney, J., Arcangeli, J., et al. (2020). A transition between the hot and the ultra-hot jupiter atmospheres. *Astron. Astrophys.* 639, A36. doi:10.1051/0004-6361/201937394

Bowesman, C. A., Shuai, M., Yurchenko, S. N., and Tennyson, J. (2021). A high-resolution line list for AlO. *Mon. Not. R. Astron. Soc.* 508, 3181–3193. doi:10.1093/mnras/stab2525

Caffau, E., Bonifacio, P., Faraggiana, R., and Steffen, M. (2011). The galactic evolution of phosphorus. *Astron. Astrophys.* 532, A98. doi:10.1051/0004-6361/201117313

Chubb, K. L., Min, M., Kawashima, Y., Helling, C., and Waldmann, I. (2020). Aluminium oxide in the atmosphere of hot jupiter WASP-43b. *Astron. Astrophys.* 639, A3. doi:10.1051/0004-6361/201937267

Clayton, D. D. (1978). "Precondensed matter: key to the early solar system,", *Paper presesnted at the conference on protostars and planets, held at the planetary science Institute*, 19. Tucson, Arizona: University of Arizona, 109–137. between January 3 and 7, 1978.). Moon and Planets. doi:10.1007/BF00896983

Colón, K. D., Kreidberg, L., Welbanks, L., Line, M. R., Madhusudhan, N., Beatty, T., et al. (2020). An unusual transmission spectrum for the sub-saturn KELT-11b suggestive of a subsolar water abundance. *Astron. J.* 160, 280. doi:10.3847/1538-3881/abc1e9

Costantini, E., Zeegers, S. T., Rogantini, D., de Vries, C. P., Tielens, A. G. G. M., and Waters, L. B. F. M. (2019). X-Ray extinction from interstellar dust - prospects of observing carbon, sulfur, and other trace elements. *Astron. Astrophys.* 629, A78. doi:10.1051/0004-6361/201833820

Danilovich, T., Gottlieb, C. A., Decin, L., Richards, A. M. S., Lee, K. L. K., Kamiński, T., et al. (2020). Rotational spectra of vibrationally excited AlO and TiO in oxygen-rich stars. *Astrophys. J.* 904, 110. doi:10.3847/1538-4357/abc079

De Beck, E., Kamiński, T., Patel, N. A., Young, K. H., Gottlieb, C. A., Menten, K. M., et al. (2013). PO and PN in the wind of the oxygen-rich AGB star Ik tauri. *Astron. Astrophys.* 558, A132. doi:10.1051/0004-6361/201321349

Decin, L., Danilovich, T., Gobrecht, D., Plane, J. M. C., Richards, A. M. S., Gottlieb, C. A., et al. (2018). Constraints on metal oxide and metal hydroxide abundances in

the winds of AGB stars: potential detection of FeO in R dor. *Astrophys. J.* 855, 113. doi:10.3847/1538-4357/aaab6a

Decin, L., Richards, A. M. S., Waters, L. B. F. M., Danilovich, T., Gobrecht, D., Khouri, T., et al. (2017). Study of the aluminium content in AGB winds using ALMA: indications for the presence of gas-phase $(Al_2O_3)_n$clusters. *Astron. Astrophys.* 608, A55. doi:10.1051/0004-6361/201730782

Deegan, M. J. O., and Knowles, P. J. (1994). Perturbative corrections to account for triple excitations in closed and open shell coupled cluster theories. *Chem. Phys. Lett.* 227, 321–326. doi:10.1016/0009-2614(94)00815-9

Dickinson, D. F. (1972). Detection of silicon monoxide at 87 GHz. *Astrophys. J. Lett.* 175, L43. doi:10.1086/180981

Doerksen, E. S., and Fortenberry, R. C. (2020). Coincidence between bond strength, atomic abundance, and the composition of rocky materials. *ACS Earth Space Chem.* 4, 812–817. doi:10.1021/acsearthspacechem.0c00029

Dunning, J., and Thom, H. (1989). Gaussian basis sets for use in correlated molecular calculations. I. The atoms boron through neon and hydrogen. *J. Chem. Phys.* 90, 1007–1023. doi:10.1063/1.456153

Firth, R. A., Bell, K. M., and Fortenberry, R. C. (2024). Formation of AlO, AlOH, and $Al(OH)_3$ in the interstellar medium and circumstellar envelopes of AGB stars. *ACS Earth Space Chem.* 8, 974–982. doi:10.1021/acsearthspacechem.3c00335

Flint, A. R., and Fortenberry, R. C. (2023). Formation and destruction of Si_6O_{12} nanostructures in the gas phase: applications to grain nucleation and water generation. *ACS Earth Space Chem.* 7, 2119–2128. doi:10.1021/acsearthspacechem.3c00207

Flint, A. R., Westbrook, B. R., and Fortenberry, R. C. (2024). Theoretical rotational and vibrational spectra data for the hypermagnesium oxide species Mg_2O and Mg_2O and Mg_2O^+. *Chem. Phys. Chem.* 25, e202400479. doi:10.1002/cphc.202400479

Fontani, F., Rivilla, V. M., Caselli, P., Vasyunin, A., and Palau, A. (2016). Phosphorus-bearing molecules in massive dense cores. *Astrophys. J. Lett.* 822, L30. doi:10.3847/2041-8205/822/2/L30

Fortenberry, R. C., and McGuire, B. A. (2024). A possible additional formation pathway for the interstellar diatomic SiS. *Astrophys. J.* 971, 101. doi:10.3847/1538-4357/ad4d94

Frisch, M. J., Trucks, G. W., Schlegel, H. B., Scuseria, G. E., Robb, M. A., Cheeseman, J. R., et al. (2016). *Gaussian 16 revision C.01*. Wallingford CT: Gaussian Inc.

Garhart, E., Deming, D., Mandell, A., Knutson, H. A., Wallack, N., Burrows, A., et al. (2020). Statistical characterization of hot jupiter atmospheres using spitzer's secondary eclipses. *Astron. J.* 159, 137. doi:10.3847/1538-3881/ab6cff

Gaudi, B. S., Stassun, K. G., Collins, K. A., Beatty, T. G., Zhou, G., Latham, D. W., et al. (2017). A giant planet undergoing extreme-ultraviolet irradiation by its hot massive-star host. *Nature* 546, 514–518. doi:10.1038/nature22392

Grosselin, D., and Fortenberry, R. C. (2022). Formation of magnesium and aluminum oxides from water and metal hydrides: creation of the smallest ruby. *ACS Earth Space Chem.* 6, 18–24. doi:10.1021/acsearthspacechem.1c00324

Győrffy, W., and Werner, H.-J. (2018). Analytical energy gradients for explicitly correlated wave functions. II. Explicitly correlated coupled cluster singles and doubles with perturbative triples corrections: CCSD(T)-F12. *J. Chem. Phys.* 148, 114104. doi:10.1063/1.5020436

Hampel, C., Peterson, K. A., and Werner, H.-J. (1992). A comparison of the efficiency and accuracy of the quadratic configuration interaction (QCISD), coupled cluster (CCSD), and brueckner coupled cluster (BCCD) methods. *Chem. Phys. Lett.* 190, 1–12. doi:10.1016/0009-2614(92)86093-W

Helgaker, T., Ruden, T. A., Jørgensen, P., Olsen, J., and Klopper, W. (2004). *A priori* calculation of molecular properties to chemical accuracy. *J. Phys. Org. Chem.* 17, 913–933. doi:10.1002/poc.841

Henry, R. B. C., Kwitter, K. B., and Balick, B. (2004). Sulfur, chlorine, and argon abundances in planetary nebulae. IV. Synthesis and the sulfur anomaly. *Astron. J.* 127, 2284–2302. doi:10.1086/382242

Herbig, G. H. (1956). Identification of aluminum hydride as the emitter of bright lines observed in Cygni near minimum light. *Publ. Astron. Soc. Pac.* 68, 204. doi:10.1086/126916

Hill, J. G., and Peterson, K. A. (2010). Correlation consistent basis sets for explicitly correlated wavefunctions: valence and core valence basis sets for Li, Be, Na, and Mg. *Phys. Chem. Chem. Phys.* 12, 10460–10468. doi:10.1039/c0cp00020e

Hony, S., Waters, L. B. F. M., and Tielens, A. G. G. M. (2002). The Carrier of the "30" the carrier of the "30" μm emission feature in evolved stars: a simple model using magnesium sulfidem Emission Feature in Evolved Stars. A Simple Model Using Magnesium Sulfide. *Astron. Astrophys.* 390, 533–553. doi:10.1051/0004-6361:20020603

Jiang, C., Chen, G., Murgas, F., Pallé, E., Parviainen, H., and Ma, Y. (2024). Confirmation of TiO absorption and tentative detection of MgH and CrH in the atmosphere of HAT-P-41b. *Astron. Astrophys.* 682, A73. doi:10.1051/0004-6361/202347989

Johnson, H. R., and Sauval, A. J. (1982). Molecules in red-giant stars. I - column densities in models for K and M stars. *Astron. Astrophys. Suppl. Ser.* 49, 77–87.

Jones, K., Morris, B. M., Demory, B.-O., Heng, K., Hooton, M. J., Billot, N., et al. (2022). The stable climate of KELT-9b. *Astron. Astrophys.* 666, A118. doi:10.1051/0004-6361/202243823

Kama, M., Shorttle, O., Jermyn, A. S., Folsom, C. P., Furuya, K., Bergin, E. A., et al. (2019). Abundant refractory sulfur in protoplanetary disks. *Astrophys. J.* 885, 114. doi:10.3847/1538-4357/ab45f8

Kamiński, T., Schmidt, M. R., and Menten, K. M. (2013). Aluminium oxide in the optical spectrum of VY Canis Majoris. *Astron. Astrophys.* 549, A6. doi:10.1051/0004-6361/201220650

Kamiński, T., Wong, K. T., Schmidt, M. R., Müller, H. S. P., Gottlieb, C. A., Cherchneff, I., et al. (2016). An observational study of dust nucleation in mira (o ceti) I. Variable features of AlO and other Al-bearing species. *Astron. Astrophys.* 592, A53. doi:10.1051/0004-6361/201628664

Karovicova, I., Wittkowski, M., Ohnaka, K., Boboltz, D. A., Fossat, E., and Sholz, M. (2013). New insights into the dust formation of oxygen-rich AGB stars. *Astron. Astrophys.* 560, A75. doi:10.1051/0004-6361/201322376

Karthikeyan, B., Rajamanickam, N., and Bagare, S. P. (2010). On the rotational temperature of AlH in sunspots. *Sol. Phys.* 264, 279–285. doi:10.1007/s11207-010-9590-8

Keller, L. P., Hony, S., Bradley, J. P., Molster, F. J., Waters, L. B. F. M., Bouwman, J., et al. (2002). Identification of iron sulphide grains in protoplanetary disks. *Nature* 417, 148–150. doi:10.1038/417148a

Kendall, R. A., Dunning, J., Thom, H., and Harrison, R. J. (1992). Electron affinities of the first-row atoms revisited. Systematic basis sets and wave functions. *J. Chem. Phys.* 96, 6796–6806. doi:10.1063/1.462569

Kirkpatrick, J. D. (2005). New spectral types L and T. *Ann. Rev. Astron. Astrophys.* 43, 195–245. doi:10.1146/annurev.astro.42.053102.134017

Knizia, G., Adler, T. B., and Werner, H.-J. (2009). Simplified CCSD(T)-F12 methods: theory and benchmarks. *J. Chem. Phys.* 130, 054104. doi:10.1063/1.3054300

Knowles, P. J., Hampel, C., and Werner, H.-J. (1993). Coupled cluster theory for high spin, open shell reference wave functions. *J. Chem. Phys.* 99, 5219–5227. doi:10.1063/1.465990

Lefloch, B., Vastel, C., Viti, S., Jimenez-Serra, I., Codella, C., Podio, L., et al. (2016). Phosphorus-bearing molecules in solar-type star-forming regions: first PO detection. *Mon. Not. R. Astron. Soc.* 462, 3937–3944. doi:10.1093/mnras/stw1918

Lewis, N. K., Wakeford, H. R., MacDonald, R. J., Goyal, J. M., Sing, D. K., Barstow, J., et al. (2020). Into the UV: the atmosphere of the hot jupiter HAT-P-41b revealed. *Astrophys. J. Lett.* 902, L19. doi:10.3847/2041-8213/abb77f

Lucas, R., and Liszt, H. S. (2000). SiO in diffuse, translucent and 'spiral-arm' clouds. *Astron. Astrophys.* 355, 327–332.

Mangan, T. P., Douglas, K. M., Lade, R. E., Gobrecht, D., Decin, L., and Plane, J. M. C. (2021). Kinetic study of the reactions of AlO with H_2O and H_2; precursors to stellar dust formation. *ACS Earth Space Chem.* 5, 3385–3395. doi:10.1021/acsearthspacechem.1c00225

Massalkhi, S., Agúndez, M., Cernicharo, J., and Velilla-Prieto, L. (2020). The abundance of S- and Si-bearing molecules in O-rich circumstellar envelopes of AGB stars. *Astron. Astrophys.* 641, A57. doi:10.1051/0004-6361/202037900

McGuire, B. A. (2018). 2018 census of interstellar, circumstellar, extragalactic, protoplanetary disk, and exoplanetary molecules. *Astrophys. J. Suppl. Ser.* 239, 17. doi:10.3847/1538-4365/aae5d2

McGuire, B. A. (2021). 2021 census of interstellar, circumstellar, extragalactic, protoplanetary disk, and exoplanetary molecules. *Astrophys. J. Suppl. Ser.* 259, 30. doi:10.3847/1538-4365/ac2a48

Neufeld, D. A., Falgarone, E., Gerin, M., Godard, B., Herbst, E., Pineau des Forêts, G., et al. (2012). Discovery of interstellar mercapto radicals (SH) with the GREAT instrument on SOFIA. *Astron. Astrophys.* 542, L6. doi:10.1051/0004-6361/201218870

Nguyen, Q. L. D., Peters, W. K., and Fortenberry, R. C. (2020). Highly-excited state properties of cumulenone chlorides in the vacuum-ultraviolet. *Phys. Chem. Chem. Phys.* 22, 11838–11849. doi:10.1039/D0CP01835J

Parnis, J. M., Mitchell, S. A., Kanigan, T. S., and Hackett, P. A. (1989). Gas-phase reactions of aluminum monoxide with small molecules. *J. Phys. Chem.* 93, 8045–8052. doi:10.1021/j100361a017

Pavlenko, Y. V., Tennyson, J., Yurchenko, S. N., Schmidt, M. R., Jones, H. R. A., Lyubchik, Y., et al. (2022). AlH lines in the blue spectrum of Proxima Centauri. *Mon. Not. R. Astron. Soc.* 516, 5655–5673. doi:10.1093/mnras/stac2588

Prieto, L. V., Cernicharo, J., Quintana-Lacaci, G., Agúndez, M., Castro-Carrizo, A., Fonfría, J. P., et al. (2015). Si-bearing molecules toward IRC+10216: ALMA unveils the molecular envelope of CWLeo. *Astrophys. J. Lett.* 805, L13. doi:10.1088/2041-8205/805/2/L13

Puzzarini, C. (2022). Gas-phase chemistry in the interstellar medium: the role of laboratory astrochemistry. *Front. Astron. Space Sci.* 8, 811342. doi:10.3389/fspas.2021.811342

Raghavachari, K., Trucks, G. W., Pople, J. A., and Head-Gordon, M. (1989). A fifth-order perturbation comparison of electron correlation theories. *Chem. Phys. Lett.* 157, 479–483. doi:10.1016/s0009-2614(89)87395-6

Ramal-Olmedo, J. C., Menor-Salván, C. A., and Fortenberry, R. C. (2021). Mechanisms for gas-phase molecular formation of neutral formaldehyde (H_2CO) in cold astrophysical regions. *Astron. Astrophys.* 656, A148. doi:10.1051/0004-6361/202141616

Ramal-Olmedo, J. C., Menor-Salván, C. A., Miyoshi, A., and Fortenberry, R. C. (2023a). Gas-phase molecular formation mechanisms of cyanamide (NH_2CN) and its tautomer carbodiimide (HNCNH) under sgr B2(N) astrophysical conditions. *Astron. Astrophys.* 672, A49. doi:10.1051/0004-6361/202245811

Ramal-Olmedo, J. C., Menor-Salván, C. A., Miyoshi, A., and Fortenberry, R. C. (2023b). Possible gas-phase synthesis of neutral malononitrile ($C_3H_2N_2$) and isocyanoacetonitrile ($NCCH_2NC$) under the upper atmospheric conditions of titan. *ACS Earth Space Chem.* 7, 1694–1712. doi:10.1021/acsearthspacechem.3c00107

Rivilla, V. M., Fontani, F., Beltrán, M. T., Vasyunin, A., Caselli, P., Martín-Pintado, J., et al. (2016). The first detections of the key prebiotic molecule PO in star-forming regions. *Astrophys. J.* 826, 161. doi:10.3847/0004-637X/826/2/161

Rogantini, D., Costantini, E., Zeegers, S. T., Mehdipour, M., Psaradaki, I., Raassen, A. J. J., et al. (2020). Magnesium and silicon in interstellar dust: X-ray overview. *Astron. Astrophys.* 641, A149. doi:10.1051/0004-6361/201936805

Sauval, A. J. (1969). Identification of SiH lines in the solar disk spectrum. *Sol. Phys.* 10, 319–329. doi:10.1007/BF00145520

Schilke, P., Benford, D. J., Hunter, T. R., Lis, D. C., and Phillips, T. G. (2001). A line survey of orion-KL from 607 to 725 GHz. *Astrophys. J. Suppl. Ser.* 132, 281–364. doi:10.1086/318951

Sharipov, A., Titov, N., and Starik, A. (2011). Kinetics of Al + H_2O reaction: theoretical study. *J. Phys. Chem. A* 115, 4476–4481. doi:10.1021/jp111826y

Sheppard, K. B., Welbanks, L., Mandell, A. M., Madhusudhan, N., Nikolov, N., Deming, D., et al. (2021). The hubble PanCET program: a metal-rich atmosphere for the inflated hot jupiter hat-P-41b. *Astron. J.* 161, 51. doi:10.3847/1538-3881/abc8f4

Siebert, M. A., Simon, I., Shingledecker, C. N., Carroll, P. B., Burkhardt, A. M., Booth, S. T., et al. (2020). A search for light hydrides in the envelopes of evolved stars. *Astrophys. J.* 901, 22. doi:10.3847/1538-4357/abac0e

Sotirovski, P. (1972). Table of solar diatomic molecular lines spectral range 4900 - 6441 Å. *Astron. Astrophys. Suppl.* 6, 85.

Sriramachandran, P., Viswanathan, B., and Shanmugavel, R. (2013). Occurrence of AlO molecular lines in sunspot umbral spectra. *Sol. Phys.* 286, 315–326. doi:10.1007/s11207-013-0264-1

Swinnen, S., Nguyen, V. S., Sakai, S., and Nguyen, M. T. (2009). Calculations suggest facile hydrogen release from water using boranes and alanes as catalysts. *Chem. Phys. Lett.* 472, 175–180. doi:10.1016/j.cplett.2009.02.078

Tachibana, S., Kamizuka, T., Hirota, T., Sakai, M., Oya, Y., Takigawa, A., et al. (2019). Spatial distribution of AlO in a high-mass protostar candidate orion source I. *Astrophys. J. Lett.* 875, L29. doi:10.3847/2041-8213/ab1653

Takigawa, A., Kamizuka, T., Tachibana, S., and Yamamura, I. (2017). Dust Formation and wind acceleration around the aluminum oxide-rich AGB star W hydrae. *Sci. Adv* 3, eaao2149. doi:10.1126/sciadv.aao2149

Tenebaum, E. D., and Ziurys, L. M. (2009). Millimeter detection of AlO $X^2\Sigma^+$: metal oxide chemistry in the envelope of VY Canis Majoris. *Astrophys. J. Lett.* 694, L59–L63. doi:10.1088/0004-637x/694/1/l59

Tenenbaum, E. D., and Ziurys, L. M. (2010). Exotic metal molecules in oxygen-rich envelopes: detection of AlOH $X^1\Sigma^+$ in VY Canis Majoris. *Astrophys. J. Lett.* 712, L93–L97. doi:10.1088/2041-8205/712/1/l93

Tennyson, J., and Yurchenko, S. N. (2017). Laboratory spectra of hot molecules: data needs for hot super-Earth exoplanets. *Mol. Astrophys.* 8, 1–18. doi:10.1016/j.molap.2017.05.002

Tinacci, L., Ferrada-Chamorro, S., Ceccarelli, C., Pantaleone, S., Ascenzi, D., Maranzana, A., et al. (2023). The GRETOBAPE gas-phase reaction network: the importance of being exothermic. *Astrophys. J. Suppl. Ser.* 266, 38. doi:10.3847/1538-4365/accae9

Turner, B. E. (1998). The Physics and chemistry of small translucent molecular clouds. X. SiO. *Astrophys. J.* 495, 804–820. doi:10.1086/305319

Tylenda, R., Crause, L. A., Górny, S. K., and Schmidt, M. R. (2005). V4332 sagittarii revisited. *Astron. Astrophys.* 439, 651–661. doi:10.1051/0004-6361:20041581

von Essen, C., Mallonn, M., Welbanks, L., Madhusudhan, N., Pinhas, A., Bouy, H., et al. (2019). An optical transmission spectrum of the ultra-hot jupiter WASP-33 b. First indication of aluminum oxide in an exoplanet. *Astron. Astrophys.* 622, A71. doi:10.1051/0004-6361/201833837

Wallace, L., Hinkle, K., and Livingston, W. (2000). An atlas of sunspot umbral spectra in the visible, from 15,000 to 25,500 cm, *Angstrom*, (3920-6664.

Wallström, S. H. J., Danilovich, T., Müller, H. S. P., Gottlieb, C. A., Maes, S., Van de Sande, M., et al. (2024). ATOMIUM: molecular inventory of 17 oxygen-rich evolved stars observed with ALMA. *Astron. Astrophys.* 681, A50. doi:10.1051/0004-6361/202347632

Werner, H.-J., Knowles, P. J., Knizia, G., Manby, F. R., and Schütz, M. (2012). Molpro: a general-purpose quantum chemistry program package. *WIREs Comput. Mol. Sci.* 2, 242–253. doi:10.1002/wcms.82

Westphal, A. J., Stroud, R. M., Bechtel, H. A., Brenker, F. E., Butterworth, A. L., Flynn, G. J., et al. (2014). Evidence for interstellar origin of seven dust particles collected by the stardust spacecraft. *Science* 345, 786–791. doi:10.1126/science.1252496

Wilson, R. W., Penzias, A. A., Jefferts, K. B., Kutner, M., and Thaddeus, P. (1971). Discovery of interstellar silicon monoxide. *Astrophys. J. Lett.* 167, L97. doi:10.1086/180769

Wöhl, H. (1971). On molecules in sunspots. *Sol. Phys.* 16, 362–372. doi:10.1007/BF00162477

Woon, D. E., Dunning, J., and Thom, H. (1993). Gaussian basis sets for use in correlated molecular calculations. III. The atoms aluminum through argon. *J. Chem. Phys.* 98, 1358–1371. doi:10.1063/1.464303

Yurchenko, S. N., Sinden, F., Lodi, L., Hill, C., Gorman, M. N., and Tennyson, J. (2017). ExoMol line lists xxiv: a new hot line list for silicon monohydride, SiH. *Mon. Not. R. Astron. Soc.* 473, 5324–5333. doi:10.1093/mnras/stx2738

Zhao, Y., and Truhlar, D. G. (2007). The M06 suite of density functionals for main group thermochemistry, thermochemical kinetics, noncovalent interactions, excited states, and transition elements: two new functionals and systematic testing of four M06- class functionals and 12 other functionals. *Theor. Chem. Acc.* 120, 215–241. doi:10.1007/s00214-007-0310-x

Ziurys, L. M., Schmidt, D. R., and Bernal, J. J. (2018). New circumstellar sources of PO and PN: the increasing role of phosphorus chemistry in oxygen-rich stars. *Astrophys. J.* 856, 169. doi:10.3847/1538-4357/aaafc6